Atmos. Chem. Phys. Discuss., 14, 31169–31201, 2014
www.atmos-chem-phys-discuss.net/14/31169/2014/
doi:10.5194/acpd-14-31169-2014

Atmospheric Chemistry and Physics Discussions
Open Access

Analysis of actinic flux profiles measured from an ozone sonde balloon

P. Wang, M. Allaart, W. H. Knap, and P. Stammes

Royal Netherlands Meteorological Institute (KNMI), De Bilt, the Netherlands

Received: 22 October 2014 – Accepted: 13 November 2014 – Published: 10 December 2014

Correspondence to: P. Wang (ping.wang@knmi.nl)

Published by Copernicus Publications on behalf of the European Geosciences Union.

Abstract

A green light sensor has been developed at KNMI to measure actinic flux profiles using an ozone sonde balloon. In total, 63 launches with ascending and descending profiles were performed between 2006 and 2010. The measured uncalibrated actinic flux profiles are analyzed using the Doubling Adding KNMI (DAK) radiative transfer model. Values of the cloud optical thickness (COT) along the flight track were taken from the Spinning Enhanced Visible and Infrared Imager (SEVIRI) Cloud Physical Properties (CPP) product. The impact of clouds on the actinic flux profile is evaluated on the basis of the cloud modification factor (CMF) at the cloud top and cloud base, which is the ratio between the actinic fluxes for cloudy and clear-sky scenes. The impact of clouds on the actinic flux is clearly detected: the largest enhancement occurs at the cloud top due to multiple scattering. The actinic flux decreases almost linearly from cloud top to cloud base. Above the cloud top the actinic flux also increases compared to clear-sky scenes. We find that clouds can increase the actinic flux to 2.3 times of the clear-sky value at cloud top and decrease it to about 0.05 at cloud base. The relationship between CMF and COT agrees well with DAK simulations, except for a few outliers. Good agreement is found between the DAK simulated actinic flux profiles and the observations for single layer clouds in fully overcast scenes. The instrument is suitable for operational balloon measurements because of its simplicity and low cost. It is worth to further develop the instrument and launch it together with atmospheric chemistry composition sensors.

1 Introduction

Atmospheric trace gases such as ozone and nitrogen dioxide are involved in a series of chemical reactions driven by solar radiation at UV wavelengths (Crutzen and Zimmermann, 1991). Actinic flux – which is the integral of the radiance over all directions, i.e. 4π solid angle – is relevant for the process of photodissociation. Clouds have a large impact on the actinic flux in the atmosphere and, consequently, on photodissociation rates (Calbó et al., 2005). Therefore, the actinic flux profile is important for the study of the change in concentration of chemically reactive components in the atmosphere and is preferably measured together with the atmospheric chemical composition. Such actinic flux profiles have been measured by means of tethered balloons and aircrafts during several campaigns.

During the Atlantic Stratocumulus Experiment (ASTEX), tethered balloon soundings were made on Santa Maria, Azores. Vilà-Guerau de Arellano et al. (1994) compared measured actinic flux profiles with simulations using a delta-Eddington model. Excellent agreement was found for fully cloudy scenes. The authors reported that the actinic flux decreased from cloud top to cloud base. At cloud top the actinic flux was higher than the clear-sky actinic flux, while at cloud base the actinic flux was lower than the clear-sky values. In the First ISCCP Regional Experiment (FIRE III) Arctic Cloud Experiment actinic fluxes were measured above sea ice in May 1998. De Roode et al. (2001) found that the actinic flux profile within clouds is nearly constant with height, except in a shallow layer below cloud top where the actinic flux revealed a large increase. The authors attributed this feature to the bright surface of sea ice (high albedo). Actinic fluxes have been measured on the ground and on an aircraft during the INSPECTRO campaign to study the effect of clouds on the spectral actinic flux in East Anglia England in 2003. Kylling et al. (2005) showed that the spectral actinic flux can be reproduced with a 1-D radiative transfer model for clear-sky and fully cloudy cases. They reported that the actinic flux (in the UV wavelength range) could be enhanced by as much as 60–100 % above clouds and reduced by 55–65 % below clouds, as compared to the clear-sky situation. Junkermann (1994) measured $J(O^1D)$ actinic flux within and above stratiform clouds and above snow surfaces from a hang glider. Palancar et al. (2011) reported extensive comparisons between aircraft-based measurements of actinic fluxes and the Tropospheric Ultraviolet-Visible (TUV) model simulations.

On the ground, UV monitoring stations usually measure spectral irradiances. The relation between the actinic flux and the irradiance was studied in several papers (e.g. Madronich, 1987; van Weele et al., 1995; McKenzie et al., 2001; Kazadzis et al., 2000).

ACPD
14, 31169–31201, 2014

In general, the actinic flux correlates well with the irradiance on the surface but the relationship depends on wavelength, surface albedo, solar zenith angle, and cloud conditions.

Most actinic flux profiles presented in the literature were measured in the lower troposphere in the UV wavelength range. Actinic flux observations at green wavelengths (about 510 nm) are more representative for photodissociation by visible light. In combination with ozone and NO_2 observations the actinic flux profile observations are useful to investigate the photostationary state relationship between NO, NO_2 and O_3 in cloudy scenes in detail (Cantrell et al., 1993; Mannschreck et al., 2004). Knowledge of the chemical inter-relationship between O_3 and NO_2 is important to better constrain their vertical profile in air quality models and in satellite retrievals of O_3 and NO_2. Although the photodissociation of nitrogen dioxide mainly in UV wavelength, good measurements and simulations of the actinic flux at visible wavelength will give some confidence with our simulations in the UV wavelengths. It was intended to be a cheap, disposable instrument and no harm for the environment. Therefore, we measured actinic flux profiles using a green light sensor attached to an ozone sonde. Another advantage of using an operational ozone sonde is the large altitude range (from surface up to 35 km) and the regularity of launching. The aims of the actinic flux profile measurements are to evaluate the impact of clouds on the actinic flux profiles and to better constrain the O_3 and NO_2 chemical inter-relationship in atmospheric chemistry models.

The cloud modification factor (CMF) is often used in the analysis of cloud effects on UV radiation (e.g. Seckmeyer et al., 1996; Mayer et al., 1998; Schwander et al., 2002; Antón et al., 2012; Mateos et al., 2014). The cloud modification factor is the ratio between UV radiation under cloudy and clear-sky conditions. The UV radiation for clear-sky scenes is calculated using the same atmospheric states as for cloudy scenes. CMF has been used to evaluate the cloud effects on irradiance, actinic flux and photolysis rate. We also use CMF in our analysis of the actinic flux profile at a green wavelength.

ACPD
14, 31169–31201, 2014

In this paper we will describe the instruments and measurements in Sect. 2. The simulation method for the actinic flux profiles is presented in Sect. 3. The results are shown in Sect. 4. Conclusions are drawn in Sect. 5.

2 Instruments and measurements

A light sensor has been developed at KNMI using a commercial green LED (Light Emitting Diode) with a diameter of 5 mm made of Gallium-Phosphide (GaP). It is mounted in the center of a 10 cm Styropor (Polystyrene) sphere. The sphere acts both as a thermal insulation and a light diffuser. The detector and amplifier are temperature stabilized at 25 °C. The instrument has been designed to have uniform response to sunlight. The point on the sphere where the LED sensor was inserted is called north pole. The senor was glued at a position in the sphere where its sensitivity to sunlight was comparable when the sphere was lit from the north or the south pole. After the instrument was completed, it was held in a beam of sunlight that would enter a single window in an otherwise dark room. The response of the instrument was checked by rotating the sphere. If it was found to be more sensitive on one side, a black permanent marker pen was used to make marks on that side. Typically it was found that the sensitivity was higher (10 % or so) on the equator compared to the poles. This process was repeated until the response of the instrument varied less than 2 % when the sphere was rotated. So the spheres have a number of black lines around the equator to make the sensitivity uniform. The light sensor is not absolutely calibrated and the measured actinic profile is in an arbitrary unit. However, before launching a light sensor, inter-comparison measurements have been performed on the ground together with one reference light sensor which is kept and not used for launching. If the reference sensor does not change with time, the actinic flux profiles measured with different sensors should be intercomparable. At present, the light sensor is mainly used to evaluate the cloud effects on actinic flux profiles. The green light sensor is chosen because it is not sensitive to ozone and water vapor absorptions, so that the impacts of clouds and aerosols on

ACPD
14, 31169–31201, 2014

the actinic fluxes can be separated from the effects of gas absorptions. The light sensor is launched together with the ozone sonde balloon and the data are transmitted during flight. The instrument weighs about 100 gram, is low cost and can be reused after recovery. The ozone sonde is launched at 11:30 UTC on every Thursday at De Bilt (5.18° E, 52.10° N), the Netherlands. The vertical velocity of the ozone sonde is typically 5 m s^{-1} and reaches an altitude of 30–35 km in 100 min. After the burst of the balloon the sonde drops back to the ground with a parachute in about 60 min. The data stream includes ascending and descending values of time, altitude, pressure, temperature, relative humidity, ozone partial pressure, and actinic flux. The trajectory of the balloon is obtained from GPS data.

3 Methods for the actinic flux profile simulations

The Doubling-Adding KNMI (DAK) radiative transfer code (De Haan et al., 1987; Stammes et al., 1989; Stammes, 2001) is used to simulate the measured actinic flux profiles. DAK is a 1-D plane-parallel radiative transfer code with a pseudo-spherical correction for solar zenith angles (SZAs) greater than 75°. Because the measurements were made at noon, the SZAs are usually smaller than 75° except in December and January. The DAK model has been used by van Weele et al. (1995) in the UV-A actinic flux calculations. The DAK simulated surface shortwave broadband irradiances have good agreement with the ground-based BSRN (Baseline Surface Radiation Network) measurements for clear-sky and overcast water clouds scenes (Wang et al., 2009, 2011). In this paper, the DAK simulations were performed for $\lambda = 550$ nm to represent the green wavelength range. Absorption by ozone is taken into account by using the shape of a climatological ozone profile and scaling it to the assimilated total ozone column at 12:00 UTC using OMI total ozone data (Eskes et al., 2003). Water vapor absorption is not taken into account in the simulations because it is weak at 550 nm.

For clear-sky scenes, aerosol optical thickness (AOT) data are taken from the SPUV sunphotometer at Cabauw (4.93° E, 51.97° N, 20 km SW of De Bilt) because AOT is

ACPD
14, 31169–31201, 2014

not measured in De Bilt. For cloudy scenes, a default AOT of 0.18 at 550 nm is used, which is close to the climatological value for Cabauw. The LOWTRAN rural aerosol profile is used, with addition of a well-mixed aerosol layer from the surface to the top of the boundary layer for clear-sky scenes. The latter is determined from the lidar measurements in Cabauw.

The cloud optical thickness, cloud phase, effective radius, cloud top height and cloud mask are obtained from the SEVIRI/MSG Cloud Physical Property (CPP) product (Roebeling et al., 2006). This product is available every 15 min. The pixel size of SEVIRI measurement is about 3 km × 6 km in the Netherlands. During one actinic flux profile measurement there are 10 SEVIRI images taken from 11:30 to 13:45 UTC. The cloud properties are selected from every SEVIRI image according to the time and geolocation of the balloon along its trajectory from launching to landing. These time and location are exactly matching between the SEVIRI images and the radiosonde. Cloud properties at 5 extra points at the start, landing, cloud top heights (1 in ascending and 1 in descending), and the highest altitude of the profile are selected at the exact geolocation but on the nearest measurement time of the SEVIRI images. The resulting 15 COT values from SEVIRI, sometimes the cloud properties are taken at two geolocations in one image, largely follow the COT variations during one profile measurement. The cloud top height is determined from the peak value in the actinic flux profile and is checked with the cloud top height in the SEVIRI data. At small SZA, the peak of the actinic flux profile is very close to the cloud top. The cloud base heights are taken from operational ceilometer measurements in De Bilt and Cabauw. The cloud scattering phase matrices were calculated using Mie theory for water droplets and using the effective radius from SEVIRI CPP data. The effective radius and cloud extinction coefficient are assumed to be constant inside the clouds. For example, if the cloud occupies 5 100 m thick layers of the atmospheric model profile and has a COT of 10, then every layer has a COT of 2. The DAK simulations are performed for 15 COT values covering the SEVIRI data. COT of 1 and 100 are also used in the DAK simulations to improve the interpolations.

ACPD
14, 31169–31201, 2014

Although there are 15 collocated COT values from SEVIRI during every actinic flux profile measurement, the COT may not be representative of the actual cloud conditions during an actinic flux profile measurement, because of retrieval uncertainty and subpixel cloud variability. The error of the COT from SEVIRI is about 15 % (http://msgcpp.knmi.nl/mediawiki/index.php/MSGCPP_product_description). Including the mismatching of the SEVIRI measurement and actinic flux profile measurement, the uncertainty of COT estimation during actinic flux profile measurement is probably larger.

In DAK, the altitude levels are specified using the atmospheric profile (height, pressure, temperature) which is taken from the ozone sonde data. In order to get high vertical resolution simulations inside the clouds, the thickness of one atmospheric profile layer is about 100 m for the cloudy atmosphere and coarser (~ 500 m) for the cloud-free atmosphere. Above 30 km, the atmospheric profile is extended using the mid-latitude summer atmospheric profile (Anderson et al., 1986). The surface albedo is assumed to be 0.15 for grass-covered surface, because the surroundings of the De Bilt site are largely covered by green grass throughout the year. The actinic flux profiles are simulated at different SZA and COT values. Then, the DAK simulated actinic fluxes are interpolated at the actual SZA and COT values along the flight track to get the best simulation for a single measured actinic flux profile.

4 Results

4.1 Actinic flux profile measurements

Actinic flux profiles were measured during 63 launches, of which 30 launches were made in 2006, 27 in 2007, 4 in 2008, and 2 in 2010. The flight trajectories were mainly between 4–9° E and 51–53° N. Most launches had one ascending profile and one descending profile; some launches had only ascending profiles while the descending

ACPD
14, 31169–31201, 2014

profiles were not received properly. In the data set there are 14 clear-sky profiles distributed over 9 days and the rest are cloudy profiles.

All the profiles are illustrated in Fig. 1a. The profiles are separated into two groups, because of a calibration issue which occurred in the year 2007. Figure 1b shows the ratio between the global irradiance measured at the ground by a pyranometer and the actinic flux at 4 m height (the lowest point of the profile) at 11:30 UTC as a function of SZA. The data points shown as filled circle are measured from 1 June to 21 December 2006. As shown in Fig. 1b, the ratio seems quite consistent in 2006 except for two outliers which are caused by very small actinic fluxes. The scatter of the points in 2006 could be due to partly cloudy scenes. This indicates that the instruments are comparable to each other and the sensors do not depend on the SZA and temperature. The calibration issue can be identified from the ratio which appears to be too variable in 2007. The irradiance vs. actinic flux ratio could be used to rule out large instrument errors before launch, however, the ratio is not suitable for the calibration of the light sensor. Therefore, in the comparison with DAK simulated profiles, the measured actinic flux profiles were normalized at 30 km and in arbitrary unit.

As shown in Fig. 1a, the actinic flux profiles have large vertical variability below 10 km because of the presence of clouds and aerosols. Above 10 km, the profiles are less variable. The ascending and descending profiles often overlap between 15 and 35 km altitude, because the sonde falls down rapidly after the burst of the balloon. The descending profiles often do not extend to the surface because of loss of radio signal at long distance.

4.2 Impact of aerosols and clouds on actinic flux profiles

Figure 2a shows four clear-sky actinic flux profiles measured on 11, 12 and 13 September 2006 and 17 April 2010. Figure 2b shows the AOT measured at Cabauw for the same days. The smallest SZA values during the actinic flux profile measurements are about 42° on 17 April 2010 and 48° for the measurements in September 2006. According to the lidar extinction coefficient profiles at Cabauw, the boundary layer heights at

11:30 UTC for the 4 days are 1.0 km (17 April 2010), 1.2, 0.5 km, and 0.7 km (11–13 September 2006), respectively. Because the AOT varies during the day (Fig. 2b) we can expect that the AOT also varies along the flight track. On 17 April 2010 the AOT is about 0.1, which is the lowest value in the four days. On this day the actinic flux profile above the boundary layer is also lower than on the other days. The AOT is about 0.3 on 12 September (12:00 UTC) and about 0.4 on 11 and 13 September. This agrees with the actinic flux measurements, namely, the actinic fluxes at 1–5 km on 11 and 13 September are slightly larger than those on 12 September. Due to the scattering by aerosols, the actinic flux is enhanced at the top of the aerosol layer and above. This further demonstrates the consistency of the instruments when the inter-comparison works well. The upper part of the actinic flux profiles (> 5 km) has no correlation with the AOT at Cabauw, because of the spatial variation of AOT and surface albedo.

The actinic flux profiles (ascending profiles only) for 6 cloudy cases are shown in Fig. 3. The actinic flux profile peaks at the upper boundary of the high relative humidity (RH) layer. Inside clouds, RH values are close to 100 %. RH values at temperatures below 0 °C are corrected to RH with respect to ice, which is larger than the measured RH with respect to water. When the balloon crosses the cloud top, the light sensor detects a sharp peak in the actinic flux profile because of the enhanced light intensity due to multiple scattering at the cloud top. Inside the cloud, the actinic flux profile decreases until the base of the cloud, and becomes relatively stable below the cloud.

The altitude dependence of the internal radiation field in a scattering atmosphere depends mainly on the optical depth τ ($\tau = 0$ at TOA and $\tau =$ the total atmospheric optical thickness at the surface) and on solar zenith angle (Stammes et al., 1989). The fact that the peak in the actinic flux is not located at the top of the atmosphere but inside the atmosphere, is due to multiple scattering. Since sunlight is incident at the top, the amount of scattered sunlight first increases going from the top downwards, reaches a maximum, and then decreases again. In first order, the flux is linear in τ at the top of the atmosphere. It has been found by Stammes et al. (1989) that for an isotropically scattering atmosphere the downward flux increases descending into the

ACPD
14, 31169–31201, 2014

atmosphere for high sun ($\mu_0 > 0.5$), but decreases for low sun ($\mu_0 < 0.5$). This finding was corroborated with multiple scattering calculations. In the field of actinic flux studies, the peak below the cloud top has been found in actinic flux calculations and in balloon measurements (Van Weele et al., 1995; Van Weele, 1996; Vilà-Guerau de Arellano et al., 1994). Also the solar zenith angle dependence has been found by these authors: in case of a high sun, solar radiation is "trapped" into the atmosphere and photons cannot escape as fast as they enter the cloud. In case of low sun (zenith angles of 52° and larger) the peak in the actinic flux was found to coincide with the cloud top. This known behavior of multiply scattered radiation inside the atmosphere is important to keep in mind when considering the AF profiles shown in this paper.

4.3 Actinic flux profiles compared with surface radiation measurements

Figure 4a shows the ratio between the actinic flux at the cloud top (the peak of the actinic flux profile) and below the cloud base close to the surface ($R_{top/base}$) as a function of the surface solar irradiance measured in De Bilt for 63 ascending profiles. Although some profiles have a calibration issue, this has no impact on ratios calculated from one profile. The ratio $R_{top/base}$ is determined by cloud optical thickness, surface albedo and solar zenith angle.

Similar to the cloud modification factor (CMF) used in UV radiation studies (e.g. Antón et al., 2012), ratios of the actinic flux profiles in cloudy scenes and clear-sky scenes are calculated at cloud top (CMF_{top}) and below the cloud base (close to the ground surface; CMF_{base}). For clear-sky scenes, the CMF is 1 by definition. In principle, the clear-sky actinic flux profile should be calculated using a radiative transfer model using an atmospheric state which is identical to the cloudy scene. Here we used the atmospheric state (temperature, pressure, aerosol optical thickness) on the clear-sky day of 11 September 2006 as a reference for all the cloudy actinic flux profiles in 2006. However, the clear-sky profiles are simulated at the same SZA as occurred for the cloudy profiles. The AOT is not available for cloudy scenes. The AOT is 0.34 on 11 September. According to the scaling factor derived from the clear-sky actinic flux profiles for 11 September 2006, the DAK simulated clear-sky profiles are converted to the same scale as the measured profiles. Otherwise, the calculated CMF would not fulfill the definition of 1 for clear-sky scenes. The simulation of the clear-sky profile is discussed in Sect. 4.4.

In Fig. 4b the CMF as a function of COT is shown for cloud top and cloud base, which we denote by CMF_{top} and CMF_{base}. The lines are simulations of CMF_{top} and CMF_{base} for SZA = 60° and 30° assuming single-layer water clouds (effective droplet radius 8 µm) with cloud top at 2.3 km and cloud base at about 1.5 km. As shown in Fig. 4b, most of the CMFs derived from the measurements are within the ranges of the simulated values. The CMF at cloud base decreases from 1 to about 0.05 with increasing COT. For the actinic flux at the surface, clouds have a shielding effect. The surface albedo is relatively small, so there is not much reflection between the cloud base and surface. Therefore, the optically thicker the clouds, the less light can penetrate the clouds. At COT close to 0, at cloud base there are some CMF_{base} values of 1.4–1.5. This indicates that the actinic fluxes in cloudy scenes are larger than for the clear-sky scenes. This could happen when broken clouds are present and 3-D effects become important.

CMF_{top} increases with increasing COT. The enhancement of the actinic flux at cloud top is caused by multiple scattering at cloud top. As illustrated by the simulated CMFs, the CMF at cloud top has stronger SZA dependence than CMF at cloud base. This may partly explain the scatter of CMF_{top}. CMF_{top} depends also on the cloud top height due to the height dependence of the clear-sky actinic fluxes. For the measured actinic flux profiles, the cloud top heights are in the range of 1–10 km. At SZA = 60°, the clear-sky actinic fluxes can increase by 10 % from 1 to 10 km and, consequently, the CMF_{top} can change by 10 %. The COT derived from SEVIRI often has a negative bias for partly cloudy scenes, especially for small-scale broken clouds. The outliers of the CMF_{top} at COT < 5 could therefore be due to the COT bias (see Fig. 4b).

If the assumed atmospheric state, especially AOT, is not the same as the actual atmospheric state, the CMF may not be 1 at COT = 0. According to our simulations,

ACPD
14, 31169–31201, 2014

the ratio of clear-sky actinic flux for AOT of 0.25 and of 0.34 is 1.04 at the surface, 0.98 at 1 km, and 0.99 at 10 km for SZA = 60°. We estimate that the uncertainty in the CMF due to the AOT uncertainty is up to 5 %.

4.4 Simulations of actinic flux profile for clear-sky scenes

As shown in Fig. 2b, the AOT on 11 September 2006 varies from 0.3 to 0.5 between 11:00 and 14:00 UTC. This may indicate that the AOT is also spatially variable. This is confirmed by MODIS AOT image which reveals a typical spatial variation in AOT between 0.2 and 0.4 for the Netherlands (see Fig. 5a and b). We used the DAK model to simulate actinic flux profiles using AOT values varying from 0 to 0.5. Then the simulated actinic flux profiles are interpolated to the measured AOT and SZA values on 11 September 2006. The simulated and measured actinic flux profiles are shown in Fig. 5c. The simulated actinic flux profile and the measured profile are normalized at 30 km with a scaling factor of 4.13 and 1.002, respectively. The simulated actinic flux profile closely follows the shape of the measured profile, although there are some small deviations. The simulated profile consists of several profiles having different AOT because the balloon moved both vertically and horizontally. In the simulated profile, when the balloon was below 1 km, the AOT was 0.5, after the balloon moved above 1 km, the AOT is 0.34. AOT values of 0.5 and 0.34 occur at different locations, not in one vertical profile. As shown in the trajectory in Fig. 5b, the measured actinic flux profile is in fact three-dimensional, because the sonde drifts away from the launch location. This feature is more significant during cloudy conditions due to the large spatial variation of cloud optical thickness.

4.5 Simulations of actinic flux profiles for fully cloudy scenes

Global irradiances derived from SEVIRI, called surface solar irradiances (SSI), are calculated using the SEVIRI COT derived from the CPP algorithm and aerosols from a monthly climatology (Greuell et al., 2013). In order to check the quality of the SE-

ACPD
14, 31169–31201, 2014

VIRI COT in the SSI calculations, we compared the SEVIRI SSI with the ground-based shortwave global irradiance measurement at De Bilt. On the 63 actinic flux profile measurement days, we compared SEVIRI SSI at 11:30 UTC with ground-based 10 min mean (11:30–11:40 UTC) pyranometer measurements of global irradiance in De Bilt. As shown in Fig. 6, the SEVIRI SSI and ground-based measurements agree well with a correlation coefficient of 0.965 and a bias of 22 $\mathrm{W\,m^{-2}}$ (for the mean SSI). This suggests that the COT from SEVIRI is of good quality and the actinic flux profiles calculated using these COTs can be realistic. The mean SSI value of 4 SEVIRI pixels and the nearest single pixel SSI are often quite different for SSI values between 200 and 800 $\mathrm{W\,m^{-2}}$. This is caused by the inhomogeneity of clouds. The cases where SSI $< 200\,\mathrm{W\,m^{-2}}$ or SSI $> 800\,\mathrm{W\,m^{-2}}$ usually correspond to fully cloudy or clear-sky scenes, respectively. Therefore, the COT of the single SEVIRI pixel that is most close to the balloon measurement time and location may not be representative of the clouds that actually determine the actinic flux profile.

The cloudy actinic flux profiles are simulated for 5 single-layer water cloud cases in 2006, of which the results are shown in Figs. 7–11. The original actinic flux profiles (without normalization) have already been shown in Fig. 3. The simulations are presented in the order of complexity of the cases. We start with the simplest case on 5 September (Fig. 7), which is followed by an optically very thick cloudy case on 15 June (Fig. 8). During these launches, the COT mainly decreased during the balloon flight. On 22 June (Fig. 9) and 10 August (Fig. 10), the COT increased after launch and decreased when the balloon was at its maximum height. On 22 December (Fig. 11) the cloud layer was low and stable but the SZA was large ($> 75^{\circ}$).

On 5 September 2006, the prevailing winds were from the west, so the balloon drifted eastwards. The SEVIRI cloud optical thickness images of 11:30 UTC and 13:00 UTC are the closest to the start and end of the ascending profile. As shown in Fig. 7a it was fully cloudy in De Bilt at 11:30 UTC when the ozone sonde was launched. The cloud optical thickness at 11:30 UTC was about 25. The clouds were optically thicker in the north-east and optically thinner south of De Bilt. At 13:00 UTC the balloon drifted

ACPD
14, 31169–31201, 2014

towards an area with COT of about 10 (see Fig. 7b). In the first 30 min, the balloon flew over clouds having similar COT, then the clouds became thinner.

The COT for the trajectory of the balloon is shown as a function of balloon altitude in Fig. 7c. The SEVIRI pixels are selected within 0.1° of the balloon lat/lon box which usually has up to 5 pixels. The number of SEVIRI pixels can be less than 5 because of missing COT data (clear-sky scene or no retrieval). Please note that the COT values in the maps are averaged over $0.1^\circ \times 0.1^\circ$ grids, while the COT values in Fig. 7c are given for single pixels.

If the balloon is above the cloud layer, variations in cloud optical thickness and cloud height will not produce sharp peaks in the actinic flux profile. However, all cloud variations along the flight track will show up in the actinic flux profile, because it includes the radiation from all directions and heights. The measured actinic flux profile in Fig. 7d shows two peaks, one at about 0.5 km, another at about 2 km. This indicates that there are two cloud layers, with cloud top heights at about 0.5 and 2 km, respectively. This is confirmed by the radar measurements at Cabauw, which show one cloud layer at 0.3–0.5 km and another cloud layer at 1–2 km.

In the simulations the clouds are assumed to be single-layer, with cloud top height at 2 km and cloud base height at 1 km. Therefore, the simulated actinic flux profile has a single peak at 2 km. The COT values used in the simulations are shown in Fig. 7c by the black line. The simulated actinic flux profile is in good agreement with the measured flux profile. Although the measured and simulated actinic flux profiles are both normalized at 30 km, this does not influence the shapes of the profiles. The consistency between the SEVIRI SSI and the ground-based global irradiance measurements suggest that the COT at De Bilt is quite representative. During the flight, the SZA changes from 29° to 34°, which has been taken into account in the simulation. The variation in the actinic flux profile shape is mainly due to variation in the COT.

The COT values and the measured and simulated actinic flux profiles for 15 June 2006 are shown in Fig. 8. The mean COT was very high, 95, at the launch in De Bilt and the actinic flux profile shows a very strong peak at 1.5 km. The balloon drifted

ACPD
14, 31169–31201, 2014

to the north, then turned west, and reached an altitude of about 30 km over a region where the COT is small. The dips in the actinic flux profile at 2 and 4 km are probably related to optically thin clouds, cloud holes, cloud shadows or clear-sky regions (Los et al., 1997).

The cloud top and base heights in simulation were at 1.5 and 0.5 km, respectively. The dips at 2 and 4 km were ignored in the simulation. As shown by the SEVIRI images of COT (Figs. 8a and b), clouds were getting thinner during the flight. The change of the measured actinic flux profile at 10 km suggests the change of COT but unfortunately there is no SEVIRI image available at this time. Therefore, the COT is extrapolated at this altitude. Above 10 km, the SEVIRI COT had to be reduced from about 30 to 20 to get a better simulation. Since the COT used in the simulation allows for closure with the measured ground-based global irradiance, the COT values used for the actinic flux profile simulation are possibly correct. In view of the uncertainty in the SEVIRI COT retrieval, the mentioned adjustment is also reasonable.

On 22 June 2006, the spatial variability in the SEVIRI COT along the balloon flight track is considerable (Figs. 9a and b). As shown in Fig. 9c, the COT decreases along the flight track and shows a large scatter. Between 10 and 20 km altitude, there are often only 2 COT values available in the 1-degree box in the SEVIRI image instead of 4 COT values, which suggests some clear-sky pixels. At launch the COT is about 30 and at 2 km altitude the COT decreases slightly. The simulated cloud top height and base height are 3 and 2 km, respectively. When the balloon passed through the cloud top, the flux profile showed a sharp peak at 3 km. The COT increased again at about 4 km, forming a broad peak in the actinic flux profile at 3–6 km. The simulated actinic flux profile follows the measured actinic flux profile shape very well. The actinic flux profile below cloud top decreases in two steps, which does not occur in the simulated profile because the extinction coefficient is assumed to be constant within the cloud.

On 10 August 2006 (Fig. 10), the clouds are optically thinner than the clouds described in the previous cases. According to SEVIRI, the COT is only about 15 at the launch in De Bilt. The main cloud layer is at 3 km. As can be seen from Fig. 10d, the bal-

ACPD
14, 31169–31201, 2014

loon went through several cloud layers between 2 and 5 km. The balloon passed over some optically thin clouds when it was at 5–10 km altitude, then the COT increased again. The simulated cloud base and top heights are 2 and 3 km, respectively. As shown in Fig. 10d the largest peak of the measured actinic flux profile and the general shape of the profile are properly simulated.

The previously described cases all have SZA smaller than 60°, so the application of a pseudo-spherical correction is not needed. However, during the actinic flux profile measurement on 21 December 2006 (Fig. 11), the SZA values ranged between 75° and 78°, therefore the pseudo-spherical correction has to be applied in the actinic flux profile simulations. Based on radar measurements in Cabauw, the cloud layer was very close to the ground surface and the cloud top height was 1 km. Although it was winter, the surface temperature was about 7 °C at the launch in De Bilt and there was no snow on the surface. As presented in Fig. 11a the SEVIRI COT is about 30 in De Bilt and relatively stable until the balloon reaches an altitude of 20 km, where the COT starts to decrease. The pixel-to-pixel variation of COT is small. Therefore, this should be a simple case to simulate. As shown in Fig. 11d, the simulated actinic profile agrees well with the measured profile shape above 10 km and below the cloud top. However, the simulated actinic flux profile from cloud top (1.5 km) to about 10 km is much smaller than the measured actinic flux profile. Apparently, some light is missing in the DAK simulations. Usually, the simulated actinic flux above clouds increases with increasing COT, but in this case the actinic flux does not increase that much at SZA $> 75°$, even if the COT is increased up to 100. It is conceivable that the full spherical geometry of the atmosphere has to be taken into account.

Another challenge for the DAK model appears to be the simulation of the actinic flux profile of 6 September 2006 (see Fig. 3e). The actinic flux profile of this day is similar to the clear-sky profiles, without sharp peaks. However, the value of the actinic flux profile above cloud top is larger than for the clear-sky scenes. According to the total sky imager data at Cabauw and MODIS Terra 1 km resolution imagery, there were many small broken clouds on this day. Since SEVIRI cannot resolve the small broken

ACPD
14, 31169–31201, 2014

clouds, the COT is quite low, about 1–3. This case probably requires a 3-D radiative transfer model for correctly simulating the actinic flux profile.

5 Conclusions

A green light sensor has been developed and launched from De Bilt on an ozone sonde balloon between June 2006 and April 2010. Several copies of this sensor were calibrated to one reference sensor to make them intercomparable, although not absolutely calibrated. The calibration failed in 2007, therefore mainly the 2006 data (ascending profiles) were used in the analysis. The instrument is not sensitive to ozone and water vapor and it is temperature-stabilized. In total there were 63 launches (one ascending profile and one descending profile per launch), of which 9 launches were made during clear-sky conditions. The other launches were made through cloudy atmospheres. The actinic flux profiles contain very little noise and the impact of clouds on the actinic flux profile could be clearly detected.

The actinic flux profile reveals an large enhancement at the cloud top. Above the cloud top, the actinic flux profile is still influenced by the clouds but the enhancement is smaller than at the cloud top. The actinic flux profile decreases from the cloud top to cloud base, almost linearly. Below the cloud base, the actinic flux profile is relatively constant, especially for the low clouds. The balloon often passed through several layers of clouds. Therefore, the actinic flux of different heights reflects different cloud conditions along the flight track. The impact of cloud is quantified by the cloud modification factor (CMF). The CMF is in the range of 1–2.3 at the cloud top and 1–0.1 at the cloud base. The CMF depends on cloud properties and SZA. The measured CMF values agree with the DAK simulated CMF, especially for cloud base CMF. The CMF at the cloud top is more complicated because sometimes the location of the cloud top can be ambiguous due to the horizontal movement of the balloon in the clouds or due to holes in vertical direction (broken clouds). For the calculation of the clear-sky actinic flux, the

ACPD
14, 31169–31201, 2014

same aerosol setting has been used for all cloudy cases, which could cause a small (5 %) uncertainty in the CMF.

The actinic flux profiles for single-layer water clouds during fully cloudy conditions were simulated using DAK. The shapes of simulated actinic flux profiles are in good agreement with the actinic flux profile measurements, except for SZA > 75°. The most important input for the simulation is the COT along the flight track, which was obtained from 15 min SEVIRI observations. However, when the optical properties of the clouds are variable at the pixel-to-pixel scale, the SEVIRI COT has to be modified to get a better simulation of the actinic flux profile. Because of the good agreement between the measured and simulated actinic flux profile shapes, it would be possible to convert the measured actinic flux profile to absolute values.

For clear-sky conditions, the most important factors determining the shape and magnitude of the actinic flux profiles are SZA, surface albedo, aerosol optical thickness and aerosol height. Using the aerosol optical thickness data for Cabauw, the measured actinic flux profiles could be simulated reasonably well. The simulations could be improved if we would have aerosol data along the flight track of the balloon.

The green light sensor that we used for the actinic flux profile measurements is cheap and stable. In combination with a ground-based irradiance measurement and retrieved COT from SEVIRI, actinic flux profiles can be calculated. The light sensor is useful for the evaluation of the impact of clouds on actinic flux profiles. Applications of measured actinic flux profiles and simultaneous ozone and NO_2 profiles (Sluis et al., 2010) in atmospheric chemistry models will be studied in the future.

Acknowledgements. We would like to thank our colleague M. van Weele (KNMI) for his comments and suggestions about the manuscript. We appreciate J. F. Meirink (KNMI) for his help with the SEVIRI CPP product, available on http://msgcpp.knmi.nl. We acknowledge the MODIS mission scientists and associated NASA personnel for the production of the MODIS AOT data. This research is supported by NWO (Netherlands Organization for Scientific Research) through the GO project "Cloud radiative forcing profile and vertical energy redistribution in the atmosphere (CRAFT)", project number ALW-GO-AO/09-22.

References

Anderson, G. P., Clough, S. A., Kneizys, F. X., Chetwynd, J. H., and Shettle, E. P.: AFGL atmospheric constituent profiles, Tech. Rep. AFGL-TR-86-0110, Air Force Geophys. Lab., Hanscom AFB, Mass, 1986.

Antón, M., Alados-Arboledas, L., Guerrero-Rascado, J. L., Costa, M. J., C Chiu, J., and Olmo, F. J.: Experimental and modeled UV erythemal irradiance under overcast conditions: the role of cloud optical depth, Atmos. Chem. Phys., 12, 11723–11732, doi:10.5194/acp-12-11723-2012, 2012.

Calbó, J., Pagès, D., and González, J.-A.: Empirical studies of cloud effects on UV radiation: a review, Rev. Geophys., 43, RG2002, doi:10.1029/2004RG000155, 2005.

Cantrell, C. A., Shetter, R. E., Calvert, J. G., Parrish, D. D., Fehsenfeld, F. C., Goldan, P. D., Kuster, W., Williams, E. J., Westberg, H. H., Allwine, G., Martin, R.: Peroxy radicals as measured in ROSE and estimated from photostationary state deviations, J. Geophys. Res., 98, 18355–18366, doi:10.1029/93JD01794, 1993.

Crutzen, P. J. and Zimmermann, P. H.: The changing photochemistry of the troposphere, Tellus B, 43, 136–151, doi:10.1034/j.1600-0889.1991.t01-1-00012.x, 1991.

De Haan, J. F., Bosma, P. B., and Hovenier, J. W.: The adding method for multiple scattering computations of polarized light, Astron. Astrophys., 183, 371–391, 1987.

De Roode, S. R., Duynkerke, P. G., Boot, W., and Van der Hage, J. C. H.: Surface and tethered-balloon observations of actinic flux: effects of arctic stratus, surface albedo, and solar zenith angle, J. Geophys. Res., 106, 27497–27507, doi:10.1029/2001JD900236, 2001.

Eskes, H., van Velthoven, P., Valks, P., and Kelder, H.: Assimilation of GOME total ozone satellite observations in a three-dimensional tracer transport model, Q. J. Roy. Meteor. Soc., 129, 1663–1681, doi:10.1256/qj.02.14, 2003.

Greuell, W., Meirink, J. F., and Wang, P.: Retrieval and validation of global, direct, and diffuse irradiance derived from SEVIRI satellite observations, J. Geophys. Res.-Atmos., 118, 2340–2361, doi:10.1002/jgrd.50194, 2013.

Junkermann, W.: Measurements of the J(O^1D) actinic flux within and above stratiform clouds and above snow surfaces, Geophys. Res. Lett., 21, 793–796, doi:10.1029/93GL03498, 1994.

Kazadzis, S., Bais, A. F., Balis, D., Zerefos, C. S., and Blumthaler, M.: Retrieval of downwelling UV actinic flux density spectra from spectral measurements of global and direct solar UV irradiance, J. Geophys. Res., 105, 4857–4864, 2000.

Kylling, A., Webb, A. R., Kift, R., Gobbi, G. P., Ammannato, L., Barnaba, F., Bais, A., Kazadzis, S., Wendisch, M., Jäkel, E., Schmidt, S., Kniffka, A., Thiel, S., Junkermann, W., Blumthaler, M., Silbernagl, R., Schallhart, B., Schmitt, R., Kjeldstad, B., Thorseth, T. M., Scheirer, R., and Mayer, B.: Spectral actinic flux in the lower troposphere: measurement and 1-D simulations for cloudless, broken cloud and overcast situations, Atmos. Chem. Phys., 5, 1975–1997, doi:10.5194/acp-5-1975-2005, 2005.

Los, A., van Weele, M., and Duynkerke, P. G.: Actinic fluxes in broken cloud fields, J. Geophys. Res., 102, 4257–4266, doi:10.1029/96JD03123, 1997.

Madronich, S.: Photodissociation in the atmosphere 1. Actinic flux and the effect of ground reflections and clouds, J. Geophys. Res., 92, 9740–9752, doi:10.1029/JD092iD08p09740, 1987.

Mannschreck, K., Gilge, S., Plass-Duelmer, C., Fricke, W., and Berresheim, H.: Assessment of the applicability of NO-NO_2-O_3 photostationary state to long-term measurements at the Hohenpeissenberg GAW Station, Germany, Atmos. Chem. Phys., 4, 1265–1277, doi:10.5194/acp-4-1265-2004, 2004.

Mateos, D., Pace, G., Meloni, D., Bilbao, J., di Sarra, A., de Miguel, A., Casasanta, G., and Min, Q.: Observed influence of liquid cloud microphysical properties on ultraviolet surface radiation, J. Geophys. Res.-Atmos., 119, 2429–2440, doi:10.1002/2013JD020309, 2014.

Mayer, B., Kylling, A., Madronich, S., and Seckmeyer, G.: Enhanced absorption of UV radiation due to multiple scattering in clouds: experimental evidence and theoretical explanation, J. Geophys. Res., 103, 31241–31254, doi:10.1029/98JD02676, 1998.

McKenzie, R. L., Johnston, P. V., Smile, D., Bodhaine, B. A., and Madronich, S.: Altitude effects on UV spectral radiance deduced from measurements at Lauder, New Zealand, and Mauna Loa Observatory, Hawaii, J. Geophys. Res., 106, 22845–22860, doi:10.1029/2001JD900135, 2001.

Palancar, G. G., Shetter, R. E., Hall, S. R., Toselli, B. M., and Madronich, S.: Ultraviolet actinic flux in clear and cloudy atmospheres: model calculations and aircraft-based measurements, Atmos. Chem. Phys., 11, 5457–5469, doi:10.5194/acp-11-5457-2011, 2011.

Roebeling, R. A., Feijt, A. J., and Stammes, P.: Cloud property retrievals for climate monitoring: implications of differences between Spinning Enhanced Visible and Infrared Imager (SEVIRI) on Meteosat-8 and Advanced Very High Resolution Radiometer (AVHRR) on NOAA-17, J. Geophys. Res., 111, D20210, doi:10.1029/2005JD006990, 2006.

Schwander, H., Koepke, P., Kaifel, A., and Seckmeyer, G.: Modification of spectral UV irradiance by clouds, J. Geophys. Res., 107, 4296, doi:10.1029/2001JD001297, 2002.

Seckmeyer, G., Erb, R., and Albold, A.: Transmittance of a cloud is wavelength-dependent in the UV-range, Geophys. Res. Lett., 23, 2753–2755, 1996.

Sluis, W. W., Allaart, M. A. F., Piters, A. J. M., and Gast, L. F. L.: The development of a nitrogen dioxide sonde, Atmos. Meas. Tech., 3, 1753–1762, doi:10.5194/amt-3-1753-2010, 2010.

Stammes, P.: Spectral radiance modelling in the UV-Visible range, in: IRS 2000: Current Problems in Atmospheric Radiation, edited by: Smith, W. L. and Timofeyev, Y. M., A. Deepak Publ., Hampton, VA, 385–388, 2001.

Stammes, P., de Haan, J. F., and Hovenier, J. W.: The polarized internal radiation field of a planetary atmosphere, Astron. Astrophys., 225, 239–259, 1989.

Wang, P., Knap, W. H., Kuipers-Munneke, P., and Stammes, P.: Clear-sky shortwave radiative closure for the Cabauw Baseline Surface Radiation Network site, the Netherlands, J. Geophys. Res., 114, D14206, doi:10.1029/2009JD011978, 2009.

Wang, P., Knap, W. H., and Stammes, P.: Cloudy-sky shortwave radiative closure for a Baseline Surface Radiation Network site, J. Geophys. Res., 116, D08202, doi:10.1029/2010JD015141, 2011.

Van Weele, M.: Effect of clouds on ultraviolet radiation, photodissociation rates of chemical species in the troposphere, Ph.D. thesis, University of Utrecht, Utrecht, the Netherlands, 1996.

Van Weele, M., Vilà-Guerau de Arellano, J., and Kuik, F.: Combined measurements of UV-A actinic flux, UV-A irradiance and global radiation in relation to photodissociation rates, Tellus B, 47, 353–364, doi:10.1034/j.1600-0889.47.issue3.6.x, 1995.

Vilà-Guerau de Arellano, J., Duynkerke, P. G., and van Weele, M.: Tethered-balloon measurements of actinic flux in a cloud-capped marine boundary layer, J. Geophys. Res., 99, 3699–3705, doi:10.1029/93JD03090, 1994.

ACPD
14, 31169–31201, 2014

Analysis of actinic flux profiles measured from an ozone sonde balloon

P. Wang et al.

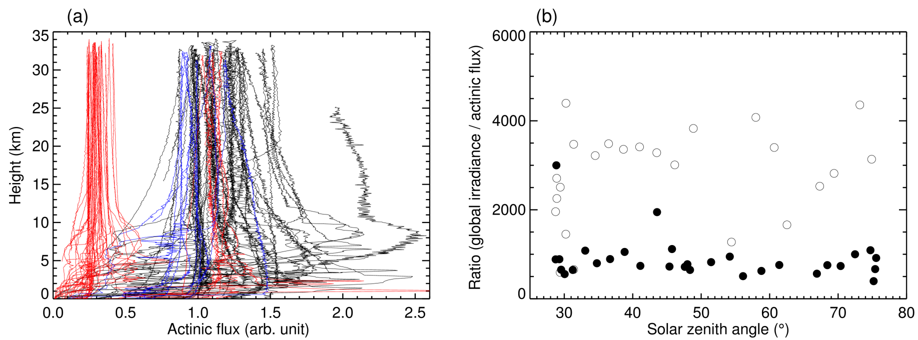

Figure 1. (a) Measured actinic flux profiles in 2006 (black lines), 2007 (red lines), 2008 and 2010 (blue lines). **(b)** Ratio between the global irradiance at the ground measured at 11:30 UTC at De Bilt and the actinic flux profile measurement at 4 m height at 11:30 UTC at De Bilt. Results for 2006 are marked as filled circles, results for 2007 are in open circles.

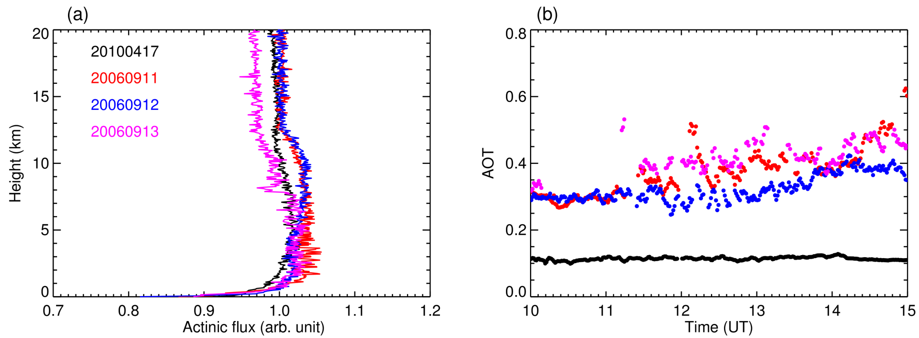

Figure 2. (a) Clear-sky actinic flux profiles measured on 11–13 September 2006 and 17 April 2010. **(b)** AOT at 501 nm measured in Cabauw for the same days. The profiles are the original measurements, not being normalized.

ACPD
14, 31169–31201, 2014

Analysis of actinic flux profiles measured from an ozone sonde balloon

P. Wang et al.

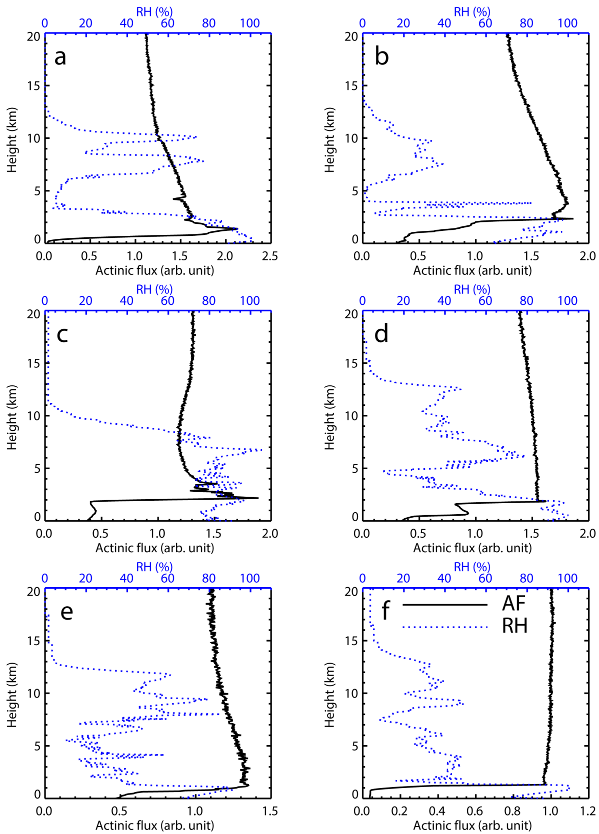

Figure 3. Actinic flux (AF) and relative humidity (RH) profiles for cloudy scenes measured on **(a)** 15 June 2006, SZA = 28.8°, **(b)** 22 June 2006, SZA = 28.7°, **(c)** 10 August 2006, SZA = 36.7°, **(d)** 5 September 2006, SZA = 45.4°, **(e)** 6 September 2006, SZA = 45.7°, and **(f)** 21 December 2006, SZA = 75.6°. The profiles are ascending measurements and are not normalized. The SZA value is at 11:30 UTC, the start of the profile.

ACPD
14, 31169–31201, 2014

Title Page
Abstract | Introduction
Conclusions | References
Tables | Figures
◀| |▶
◀ ▶
Back | Close
Full Screen / Esc
Printer-friendly Version
Interactive Discussion

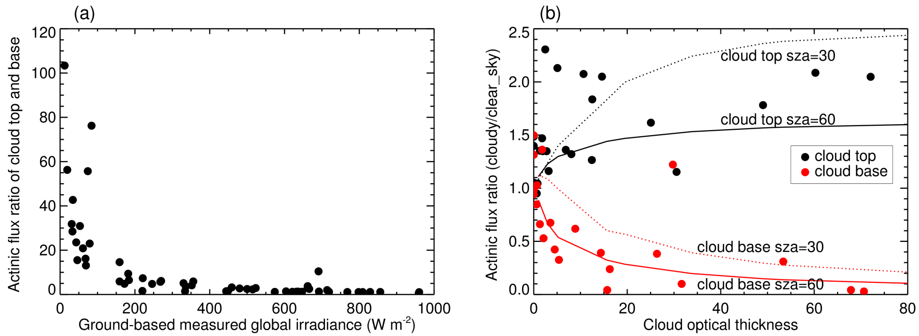

Figure 4. (a) Ratio between the measured actinic fluxes at cloud top and at cloud base vs. the measured global irradiance at the surface, for all data. **(b)** Ratio between measured actinic fluxes of cloudy and clear-sky scenes (CMF) at cloud top (black) and cloud base (red) vs. SEVIRI cloud optical thickness at 11:30 UTC for data in 2006. The dots are measurements, the lines are simulations for CMF.

ACPD
14, 31169–31201, 2014

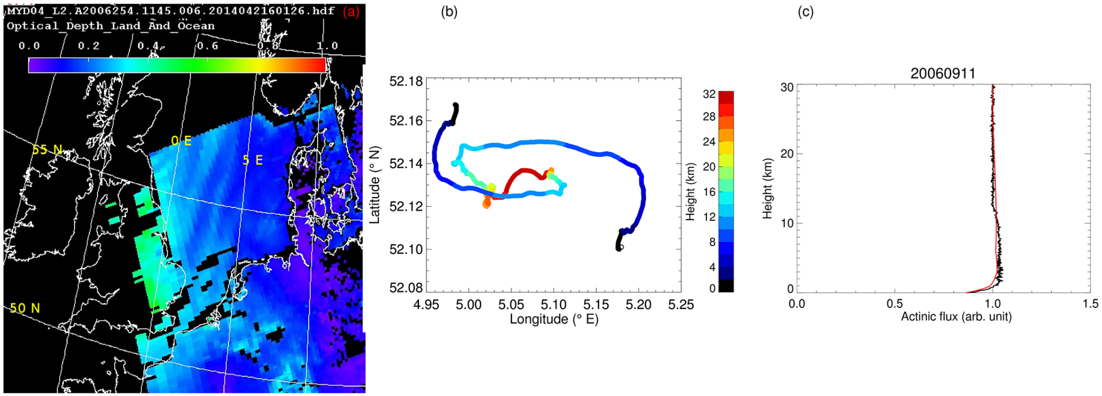

Figure 5. Clear-sky case on 11 September 2006. **(a)** MODIS AOT image at 11:45 UTC. **(b)** Trajectory of the balloon, with its height indicated by color. The location of De Bilt is marked with a circle. **(c)** Measured actinic flux profile and simulated actinic flux profile.

ACPD
14, 31169–31201, 2014

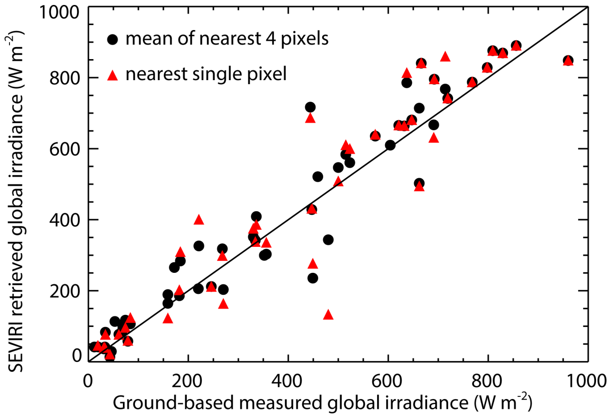

Figure 6. Scatter plot of SEVIRI retrieved global irradiance at the surface (surface solar irradiance, SSI) vs. ground-based measured global irradiance at 11:30 UTC at De Bilt on all 63 actinic flux profile measurement days. The black line is the one-to-one line. The black dots indicate the mean SSI of all SEVIRI pixels in a 0.1° × 0.1° (latitude × longitude) grid box. The red triangles indicates the nearest single pixel SSI in the grid box.

ACPD
14, 31169–31201, 2014

Analysis of actinic flux profiles measured from an ozone sonde balloon

P. Wang et al.

Title Page
Abstract Introduction
Conclusions References
Tables Figures
◂◂ ▸▸
◂ ▸
Back Close
Full Screen / Esc
Printer-friendly Version
Interactive Discussion

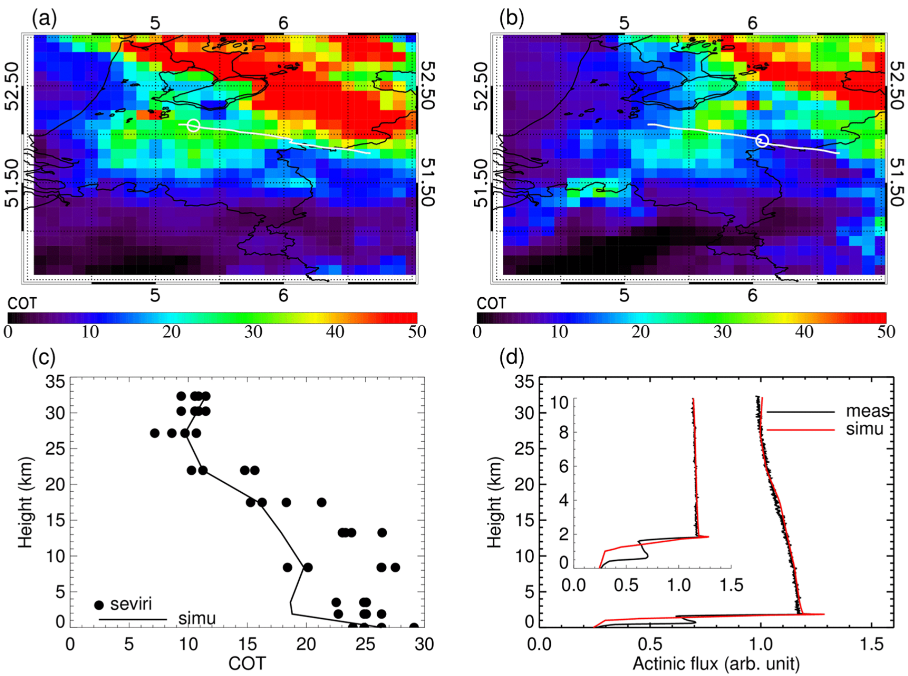

Figure 7. Cloudy sky case on 5 September 2006. **(a)** SEVIRI cloud optical thickness image at 11:30 UTC (balloon launch) and **(b)** at 13:00 UTC (balloon maximum height). The flight track of balloon is indicated as a white line. The location of balloon at the time the SEVIRI image is taken is indicated as a white circle. **(c)** SEVIRI single pixel cloud optical thickness values in $0.1^{\circ} \times 0.1^{\circ}$ (latitude × longitude) boxes along the trajectory of the balloon (dots) as a function of the height of the balloon. The COT values used in the simulations are connected by the black line. **(d)** Measured actinic flux profile and simulated actinic flux profile (both normalized at 30 km altitude, respectively). The actinic flux profile is also shown zoomed-in at 0–10 km.

ACPD
14, 31169–31201, 2014

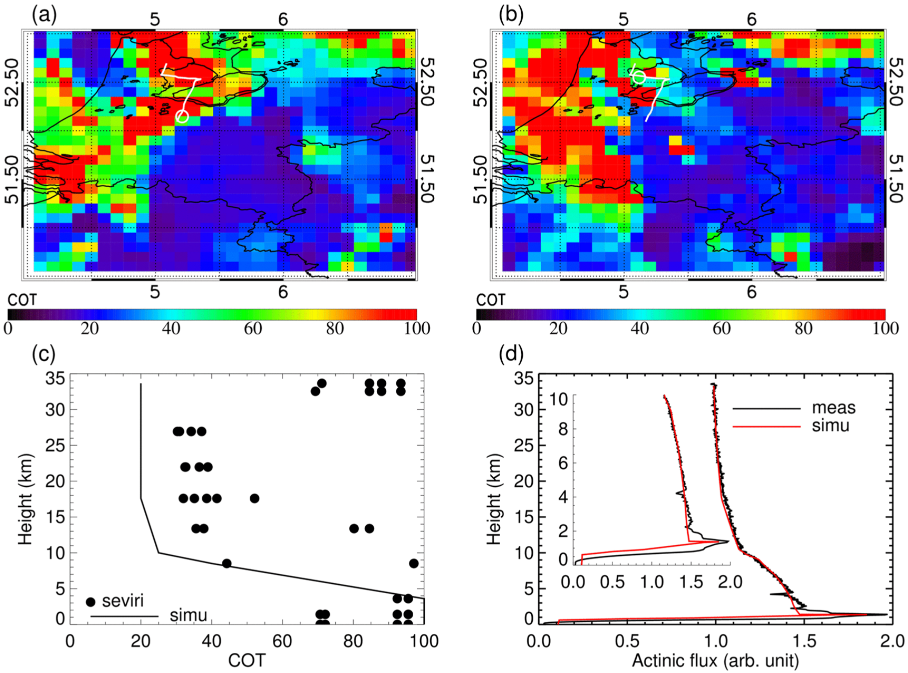

Figure 8. Same as Fig. 7 but for 15 June 2006.

ACPD
14, 31169–31201, 2014

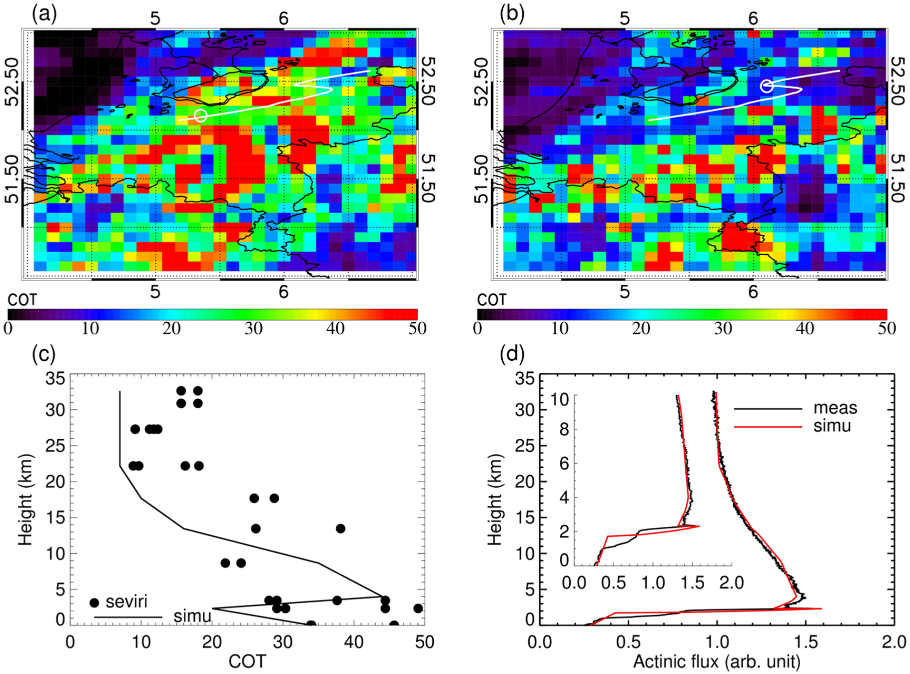

Figure 9. Same as Fig. 7 but for 22 June 2006.

ACPD
14, 31169–31201, 2014

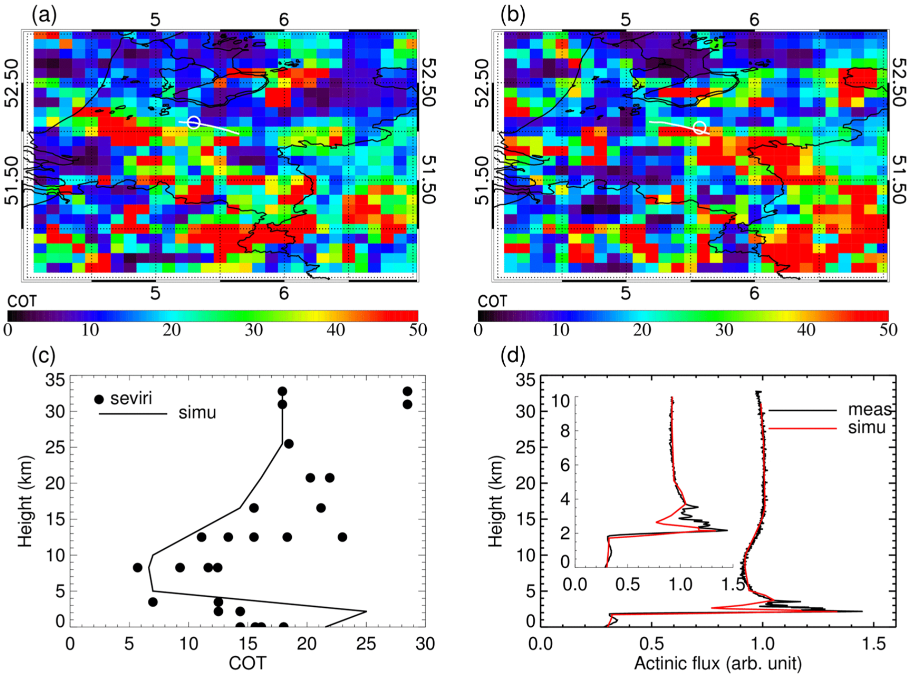

Figure 10. Same as Fig. 7 but for 10 August 2006.

ACPD
14, 31169–31201, 2014

Analysis of actinic flux profiles measured from an ozone sonde balloon

P. Wang et al.

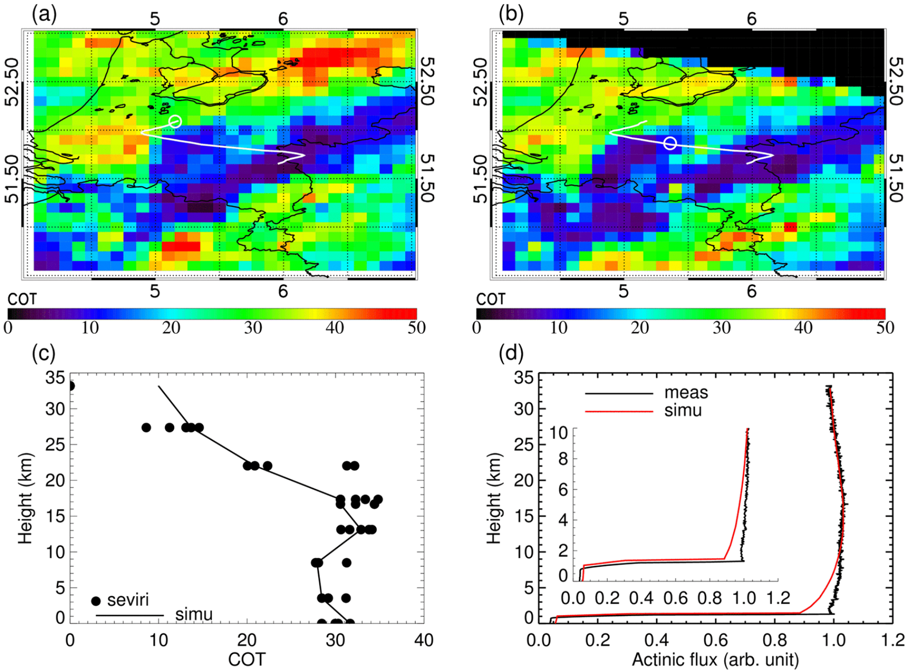

Figure 11. Same as Fig. 7 but for 21 December 2006. **(b)** The SEVIRI image was acquired at 12:45 UTC instead of 13:00 UTC.

ACPD
14, 31169–31201, 2014